Seismic-driven pore and fracture pressure prediction in the Permian Basin

Ahmed Mohamed [1], Kit Clemons[2], Vishnu Pandey[1], Bertrand Six[1], Kevin Chesser[1], and Vivek Swami[1]*
[1]CGG, [2]LARIO Oil & Gas

Summary

Unconventional reservoirs cannot be characterized by relying on the juxtaposition of single-attribute analysis. To understand their complexity, many correlated static and dynamic reservoir properties need to be carefully and quantitatively analyzed as part of integrated multidisciplinary studies. The goal of quantitative interpretation is to predict reservoir properties away from control points in order to improve vertical and lateral well placement to maximize stimulated reservoir volume (SRV) and productivity. The dense lateral spacing of three-dimensional (3D) seismic lends itself to estimating reservoir properties in 3D. Therefore, prediction of elastic attributes from seismic amplitude away from wells is common practice. However, transforming these elastic properties into geomechanical and other reservoir properties requires integration of multiple data sets (e.g., wireline logs, core, and cuttings) at various scales. Integration of all of this information is essential for de-risking seismic amplitude-supported interpretations. This study demonstrates this approach and the methods used to help predict geomechanical properties in 3D space, away from well control. The computed geomechanical volumes (pore pressure (Pp), fracture pressure (Fp), and minimum horizontal stress (SHmin)) were used to pick intermediate casing points (IPCs) and to predict recommended maximum and minimum mud weights, both of which provided significant capital savings in casing design and/or lost bottom hole assemblies (BHAs).

Introduction

Prospectivity of unconventional reservoirs is governed by a complex set of dynamic and static reservoir properties, and therefore requires a multidisciplinary approach to reach an adequate understanding of key subsurface variations. One such integrated technique is quantitative interpretation (QI), which, as the name implies, is used to quantify various reservoir parameters, including elastic, mineralogical, lithological, geochemical, geomechanical, and anisotropic properties over a 2D line or 3D volume.

This study utilizes multiclient PSTM gathers acquired in Martin County, Texas for inversion. A new workflow, based on rock physics, statistics, and empirical methods, integrates mineralogical, geochemical, geomechanical, and petrophysical properties in order to reconcile sampling differences among data sets. Initial analysis is one-dimensional (1D), focused on data-rich control at wells, and is then extended to 3D using seismic data in order to delineate targeted reservoirs, as depicted in Figure 1.

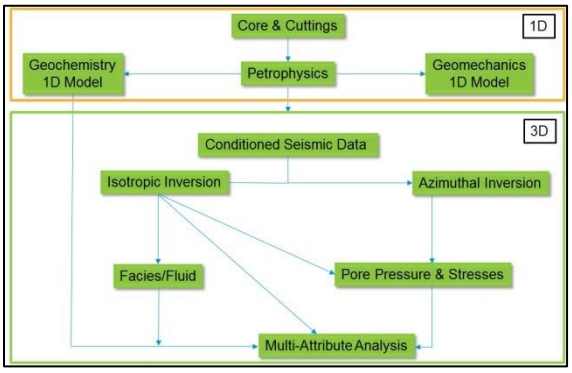

Figure 1: Schematic diagram of integrated workflow

Method

1D Analysis

The primary objective of the 1D analysis was to generate high-quality elastic, petrophysical, geomechanical, and geochemical properties at control wells, and then use these parameters to calibrate and validate corresponding 3D seismic-derived attributes.

The first step in 1D analysis was to apply a rigorous check to identify poor-quality data. Missing or erroneous elastic logs (namely P-sonic, S-sonic, and density) were ultimately replaced with rock physics analogs. Petrophysical properties, such as porosity, saturation, and mineral volumes, were estimated prior to this step and calibrated with sample analysis from drill cuttings or cores using SEM-EDS technology. Next, formation Pp was estimated using modified assumptions of Eaton's method (1976) (e.g., P-velocity (Vp) slower than a local trend associated with hydrostatic pressure is an indication of overpressure). Estimated Pp was calibrated with known values measured during well tests (Figure 2). This method accounts for significant lithology and porosity variation in unconventional mudrocks and corrects for these effects when estimating deviation (ΔVp) from the normal pressure trend (Yale et al., 2018). The modified Eaton-Yale lithology-porosity workflow comprises Voigt-Reuss-Hill (VRH) and Vp-modulus rock physics models, which are used to correct in-situ Vp for lithology variation. The

10.1190/segam2019-3216607.1

lithology-correction workflow generates a Biot's coefficient effective stress parameter in each well. The porosity correction applied to in-situ Vp is calculated using the critical porosity method (Mavko et al., 1991), where the Vp modulus and porosity are related as follows:

$$Vp_{mod} = Vp_{mod-VRH} * (1 - \phi/\phi c) \ , \qquad (1)$$

where ϕ_c is the critical porosity and $Vp_{mod\text{-}VRH}$ is the average Vp modulus of all minerals at the target depth using the VRH model. After correcting measured Vp for porosity and lithology and computing Biot's coefficient, Pp is computed as follows:

$$P_p = OBP - (OBP - \alpha P_{hyd}) * C * \left(\frac{V_{p-meas-porocorr}}{V_{p-NPT-lithcorr}}\right)^{EE} / \alpha, \quad (2)$$

where OBP is overburden pressure, P_{hyd} is hydrostatic pressure, and $V_{p\text{-}meas\text{-}porocorr}$ is the porosity corrected measured Vp. $V_{p\text{-}NPT\text{-}lithcorr}$ is the lithology corrected Vp-NPT curve fit, where NPT is the normal pressure trend and α is Biot's coefficient. In Equation 2, C is a calibration factor and EE is the Eaton exponent.

Estimated Pp was calibrated using data from DFITs, DSTs, shut-ins, and mud-weights (MW). The EE and NPT calibration factors were adjusted during the workflow to match measured Pp values.

Dynamic anisotropic geomechanical properties, including Young's modulus and Poisson's ratio, were estimated using cross-dipole logs, lithology logs, porosity, water saturation, bulk density, and calibrated Pp. They were transformed into static properties using empirical models based on core measurements, and were then used to predict in-situ stresses, assuming HTI media (Figure 2). In-situ stress was based on the Eaton-Schoenberg equation, in which overburden stress is found by mathematical integration of bulk density logs (Schoenberg, 1980). Image logs were used in the workflow to discriminate natural fractures from drilling-induced fractures, and drilling reports were used to estimate effective circulating density (ECD). ECD establishes lower limits of in-situ stress for drilling-induced fractures. Tectonic strain/stress was also adjusted during the calibration process to match known stress profiles calculated from Fp recorded from well tests (Figure 2).

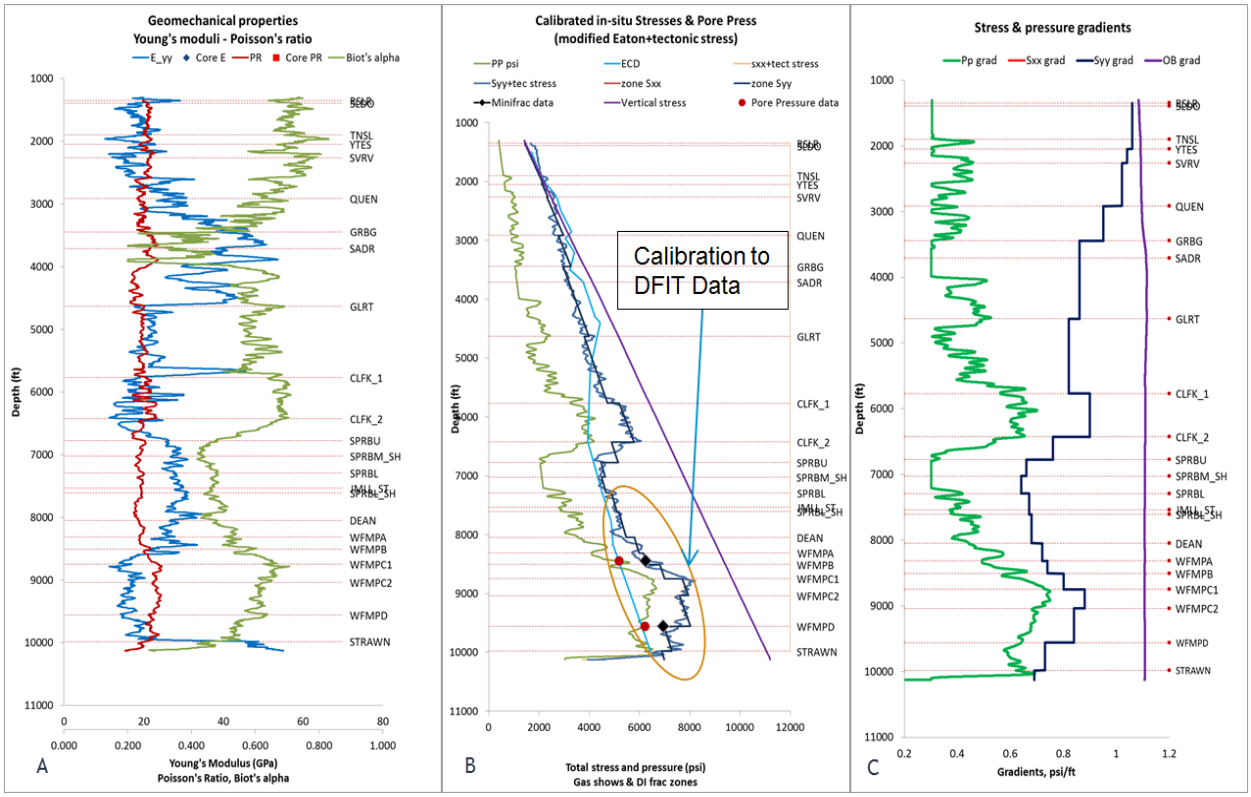

Figure 2: (a) Geomechanical properties-Young's modulus, Poisson's ratio and Biot's coefficient – calibrated to laboratory measurements, (b) Pp, horizontal and vertical stresses – calibrated to DFITs and (c) Pp and stress gradients.

10.1190/segam2019-3216607.1

3D Analysis

Following the methods applied to the 1D model, reservoir properties, including Pp and in-situ stresses, were predicted in 3D. Seismic was used to estimate reservoir properties (elastic, petrophysical, anisotropic, and geomechanical attributes) via seismic inversion and artificial neural network (ANN) algorithms. During the process, well data was used to cross-check, calibrate, and verify isotropic and anisotropic inversion results. A sparse-spike, isotropic seismic inversion (Debeye and Riel, 1990) was performed to estimate P-impedance, S-impedance, and Vp/Vs in the reservoir space (Figure 3). Accurate density was not obtained from this inversion due to coverage angle limitations, even though it is required in calculations of overburden stress, effective vertical stress, and Young's modulus. Density, therefore, was estimated in 3D from inversion products and other seismic attributes using ANN. Porosity, saturation, and mineralogy (e.g., quartz volume) were also estimated in this manner (Winter et al., 2018). Using static/dynamic relationships from the 1D model, static Young's modulus and Poison's ratio were estimated from the corresponding dynamic volumes. Isotropic inversion results, together with 1D Pp analysis, were used to compute the 3D Pp volume. Biot's coefficient was obtained by extrapolating well data, while inverted Vp was corrected for lithology and porosity. These corrections transformed inverted Vp into two volumes: [Vp-inv-porocorr] and [Vp-NPT-lithocorr]. The EE and NPT calibration factors, obtained in the 1D analysis were then applied to calibrate the 3D volume.

Prediction of reservoir anisotropic parameters was achieved by integrating full-azimuth seismic data and an anisotropic 1D mechanical earth model (MEM) through anisotropic inversion (Bakulin et al., 2000; Downtown and Roure, 2010; Zhang and Mesdag, 2016). Magnitude of anisotropy (Figure 4) and orientation were found first, then cross-checked at well locations against the anisotropic 1D model and image logs.

Linear slip deformation (LSD) theory (Schoenberg and Sayers, 1995) was applied to constrain the anisotropic solution-space and to estimate fracture parameters (i.e., normal and tangential weaknesses, calibrated with the 1D model at well locations). Next, the two principal horizontal stress components were calculated in 3D as functions of static Young's modulus and Poisson's ratio (from isotropic inversion), and normal compliances (from anisotropic inversion; Gray el al., 2012). Effective stresses from Gray et al. (2012) were modified to yield total stresses by introducing Biot's effective stress term and Pp. Finally, Fp was estimated. The resulting 3D Fp volume was then calibrated against the 1D model obtained during the 1D analysis (Figure 5).

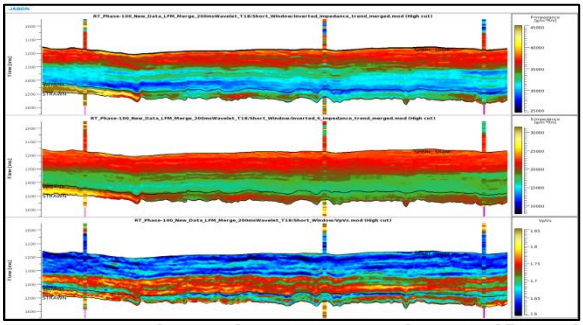

Figure 3: Inverted P-impedance (top), S-impedance (middle), and Vp/Vs (bottom) overlaid with corresponding elastic attributes computed from wireline logs. Blue colors indicate low values and gold colors show high attribute values.

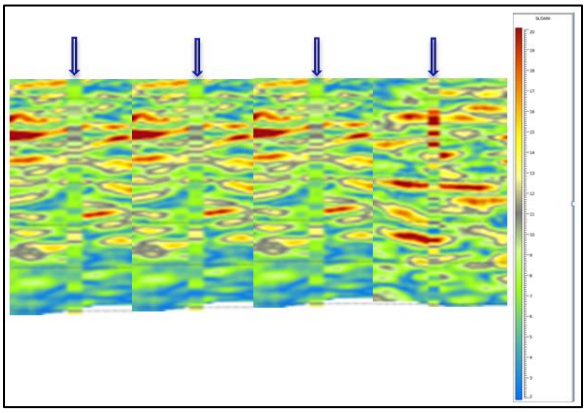

Figure 4: Inverted magnitude of anisotropy (from anisotropic inversion) around four key wells overlaid with magnitude of anisotropy from well data. Arrows show the locations of wells. Blue colors indicate low anisotropy and red colors indicate high anisotropy.

Application

ICPs protect against borehole caving and enable the use of drilling muds with variable density (mud weight) necessary for wellbore stability. Higher mud weight is required to control high pressure, while weak formations must be protected to prevent lost circulation or stuck pipe. Hence, setting the ICPs correctly is paramount to selecting the optimal mud weight for safe drilling. Figure 5 exhibits a 3D display of the Fp volume and wellbores. Two wells sustained a failure at the casing shoe, leading to loss of the BHAs. The ICPs in these wells precluded the use of heavy mud during subsequent drilling because they were placed in formations with low Fp. These ICPs were picked prior

10.1190/segam2019-3216607.1

to the delivery of seismic-derived Fp. Figure 6 shows a crossplot between seismic-predicted SHmin versus mud weight in SHmin equivalent ($r^2 = 0.74$). Post-mortem analysis of the failed wells suggests Fp was correctly estimated (close to the 1:1 line) by seismic. Nonetheless, the ICPs could have been picked in zones with higher Fp to allow for heavier mud.

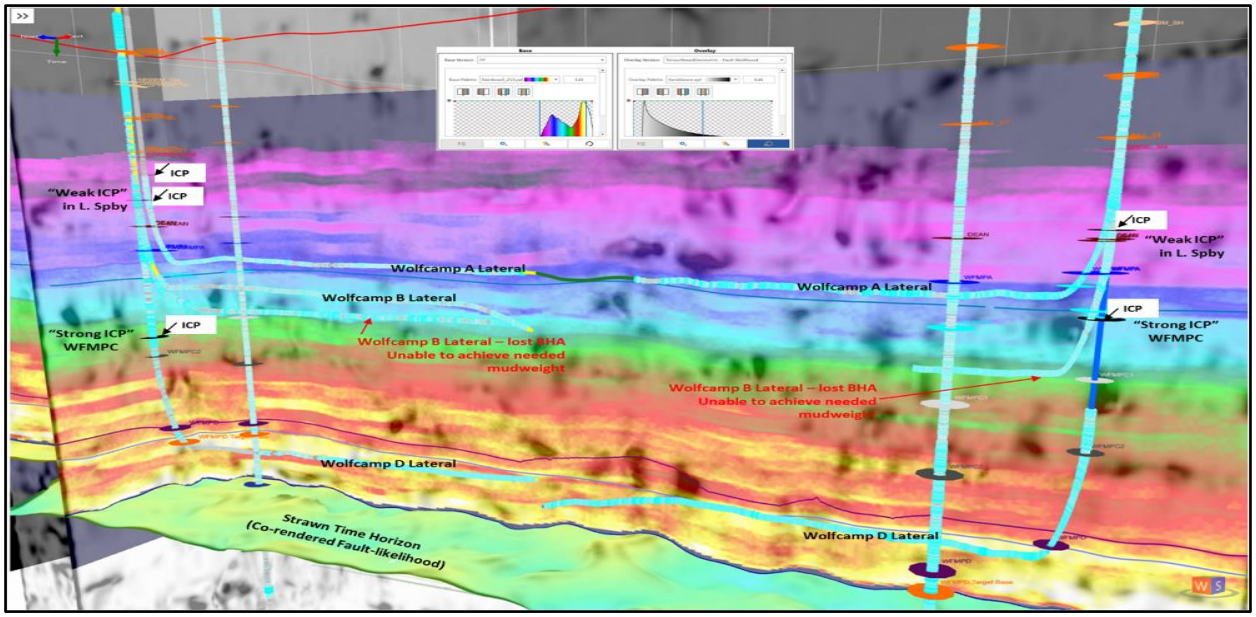

Figure 5: Fp volume co-rendering fault likelihood attributes. Purple color indicates lower values of Fp while the red, yellow, and white indicate large values of Fp. Marker tops and ICPs are displayed along the wellbores. Red arrows indicate wells with lost BHA.

Following delivery of inversion products, the operations geologist consulted the Fp volume to select ICPs in new wells (I-L; Figure 5), resulting in better well design and less downtime from drilling issues.

Conclusions

Integration of data from multiple sources enabled rock and reservoir property mapping of subsurface variations vertically and laterally away from well control. Integrated analysis increased the accuracy, detail, coverage, and overall value of the results. Geomechanical parameters generated from elastic properties and in-situ stress analysis led to better understanding of drilling, completion, and stimulation designs. In this case, Pp and Fp were used to successfully pick ICPs ahead of the drill bit, leading to more efficient drilling and significant capital savings through reduction of lost BHAs.

Acknowledgements

The authors thank Lario Oil and Gas, Inc. and CGG Multi-Client New Ventures for permission to use data and publish this abstract, and for critical contributions to its content.

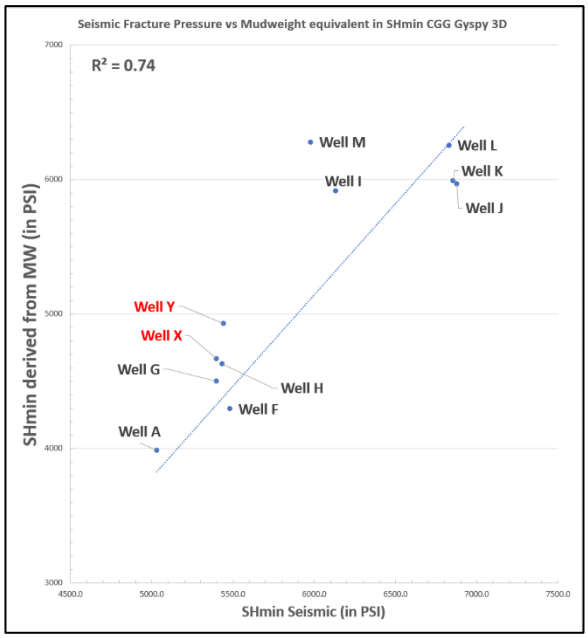

Figure 6: Seismic-derived SHmin versus SHmin derived from MW used during drilling. The two wells plotted in red were drilled prior to the delivery of the seismic-derived SHmin and sustained shoe failure.

10.1190/segam2019-3216607.1

REFERENCES

Bakulin, A., V., Grechka, and I., Tsvankin, 2000, Estimation of fracture parameters from reflection seismic data—Part I: HTI model due to a single fracture set: Geophysics, **65**, 6788–1802, doi: https://doi.org/10.1190/1.1444863.

Debeye, H. W. J., and P., Riel, 1990, LP norm deconvolution: Geophysical Prospecting, **38**, 481–403, doi: https://doi.org/10.1111/j.1365-2478.1990.tb01852.x.

Downton, J., and B., Roure, 2010, Azimuthal simultaneous elastic inversion for fracture detection: 80th Annual International Meeting, SEG, Expanded Abstracts, 263–267, doi: https://doi.org/10.1190/1.3513389.

Eaton, B. A., 1976, Graphical method predicts geopressures worldwide: World Oil, **183**, 182–188.

Gray, D., P., Anderson, J., Logel, F., Delbecq, D., Schmidt, and R., Schmid, 2012, Estimation of stress and geomechanical properties using 3D seismic data: First Break, **30**, 39–68, doi: https://doi.org/10.3997/1365-2397.2011042.

Mavko, G., T., Mukerji, and J., Dvorkin, 2009, Rock physics handbook: Cambridge University Press.

Schoenberg, M., 1980, Elastic wave behavior across linear slip interfaces: The Journal of the Acoustical Society of America, **68**, 1516–1521, doi: https://doi.org/10.1121/1.385077.

Schoenberg, M., and C., Sayers, 1995, Seismic anisotropy of fractured rock: Geophysics, **60**, 104–211, doi: https://doi.org/10.1190/1.1443748.

Winter, O., A., Mohamed, A., Leslie, G., Castillo, H., Odhwani, T., Coulman, F., Brito, A., Perez, V., Pandey, C., Marin, and C. V., Ly, 2018, Bringing multidisciplinary geosciences into quantitative inversion: A Midland Basin case study: The Leading Edge, **37**, 373–181, doi: https://doi.org/10.1190/tle37030173.1.

Yale, D., A., Perez, and R., Raney, 2018, Novel pore pressure prediction technique for unconventional reservoirs: Unconventional Resources Technology Conference, URTec-2901731.

Zhang, M., and P., Mesdag, 2016, Full data-driven azimuthal inversion for anisotropy characterization: 86th Annual International Meeting, SEG, Expanded Abstracts, 403–407, doi: https://doi.org/10.1190/segam2016-13688732.1.